Lattice dynamics of $CH(NH_2)_2PbI_3$ and $CH(NH_2)_2SnI_3$ investigated by inelastic x-ray scattering and comparison of their elastic properties

H. Tamatsukuri [1,2,*], Y. Murakami,[2,3] N. Saito [4] N. Ohashi [4,3] and S. Tsutsui [5,6]

[1]*Materials and Life Science Division, J-PARC Center, Japan Atomic Energy Agency, Tokai, Ibaraki 319-1195, Japan*
[2]*Condensed Matter Research Center (CMRC) and Photon Factory, Institute of Materials Structure Science,*
High Energy Accelerator Research Organization (KEK), Tsukuba, Ibaraki 305-0801, Japan
[3]*Materials Research Center for Element Strategy, Tokyo Institute of Technology, Yokohama, Kanagawa 226-8503, Japan*
[4]*National Institute for Materials Science (NIMS), Tsukuba, Ibaraki 305-0044, Japan*
[5]*Japan Synchrotron Radiation Research Institute (JASRI), SPring-8, Sayo, Hyogo 679-5198, Japan*
[6]*Institute of Quantum Beam Science, Graduate School of Science and Engineering, Ibaraki University, Hitachi, Ibaraki 316-8511, Japan*

Using the inelastic x-ray scattering (IXS) technique, we investigate the lattice dynamics of inorganic–organic hybrid iodide perovskites FAPbI₃ and FASnI₃ (FA ≡ $CH(NH_2)_2$, formamidinium) in their cubic α phase and tetragonal β phase. We find that the IXS spectra of FASnI₃ are highly broad at all momentum points, as has been widely observed in the Pb-based halide perovskites. The speeds of sound (phonon group velocities) and absolute values of elastic constants of FASnI₃ are smaller than those of FAPbI₃ in both phases. In addition, no significant difference in the phonon lifetimes of FAPbI₃ and FASnI₃ is observed. These results correlate better with the reported tendency that the lattice thermal conductivity of ASnX₃ is lower than that of APbX₃. We discuss that our results also favor the up-conversion mechanism by acoustic phonons in the phonon bottleneck effect for the long lifetime of hot carriers.

I. INTRODUCTION

Over 30 years, metal halide perovskites have been extensively studied as candidate materials for photovoltaic, optoelectronic, and thermoelectric applications [1–5]. They have the general chemical formula AMX₃, where A^+ = Cs^+, $MA^+ \equiv CH_3NH_3^+$ (methylammonium), or $FA^+ \equiv CH(NH_2)_2^+$ (formamidinium); M = Pb^{2+} or Sn^{2+}; $X^- = I^-$, Br^-, or Cl^-.

The ultralow thermal conductivity and the coherent band transport in this system are helpful for thermoelectric applications [3]. These properties are attributed to the metal halide perovskites that belong to "phonon glass electron crystal" materials [6]. The concept of the phonon glass electron crystal indicates that charge transport is bandlike and phonon transport is diffusive [6]. The phonon glass character appears to stem from a rattlinglike motion of the A^+ ion [7,8] and/or the dynamical disorder of the MX_6 octahedron [9,10]. These motions would cause phonon–phonon scattering, especially acoustic phonons that are the chief causes of dissipation of heat, and interfere with the thermal transport, leading to the low lattice thermal conductivity in this system [7,8,11].

The phonon glass concept is vital for the photovoltaic and the optoelectronic properties of metal halide perovskites [7], although it was initially introduced to search for suitable candidates for efficient thermoelectric materials. Regarding photovoltaics and optoelectronics, such as solar cells and light

emitters, it is crucial to understand the reason for the long lifetime of hot carriers in these materials [1,2]. Several studies have highlighted that the phonon glass character promotes the large polaron formation, which protects charge carriers from the scattering with charged defects and other charge carriers, elongating their lifetime [7,12–17]. Furthermore, at higher carrier densities, a phonon bottleneck that further slows the cooling of the hot carriers occurs in the metal halide perovskites [18–23]. As a possible origin for the phonon bottleneck effect, an up-conversion hypothesis has been proposed [20]: if phonon propagation, especially acoustic phonons, is prevented by, for example, anharmonic phonon–phonon interactions, then their energy re-excites low-energy phonons that reheat the carries, leading to the long lifetime of the hot carriers. The phonon glass character might be beneficial for the phonon bottleneck effect because the up-conversion of acoustic phonons would easily occur due to the suppression of thermal transport and dissipation [24].

Recently, ASnX₃ have been attracted to avoid using the toxic element Pb [4,25–27]. Since the direct bandgap and the carrier mobilities of ASnX₃ tend to be narrower and higher, respectively, than those of their Pb-based counterparts [25–27], they are potentially more desirable for photovoltaics and optoelectronics. An extremely long hot carrier lifetime has been reported in FASnI₃ thin films, where the phonon bottleneck effect and the up-conversion mechanism as its origin are considered to play a critical role [22,24]. Moreover, the thermal conductivity of MASnI₃ is the lowest among the metal halide perovskite families [3,28]. Information on the lattice dynamics and mechanical properties of ASnX₃ is

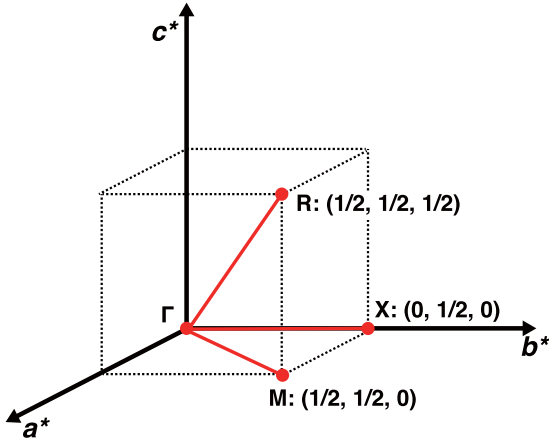*Contact author: hiromu.tamatsukuri@j-parc.jp

FIG. 1. A schematic Brillouin zone of a cubic lattice. High-symmetry points are also shown.

crucial for understanding their fascinating material performances based on the "phonon glass."

This study investigates the lattice dynamics of FAPbI$_3$ and FASnI$_3$ in their cubic α and tetragonal β phases. The speeds of sounds (phonon group velocities) and elastic constants of FASnI$_3$ are smaller than those of FAPbI$_3$ in both phases, whereas no significant difference in the phonon lifetimes (the reciprocal of the width of the phonon peaks) of FAPbI$_3$ and FASnI$_3$ is observed. These results correlate better with the lower thermal conductivity of ASnX$_3$ than that of APbX$_3$ [28]. Considering the reported assumption that the up-conversion of acoustic phonons easily occurs in materials with lower lattice thermal conductivity, our results favor the up-conversion mechanism by acoustic phonons in the phonon bottleneck effect for the long lifetime of hot carriers.

FAPbI$_3$ and FASnI$_3$ crystallize in the cubic structure with the space group $Pm\bar{3}m$ at room temperature [29–32]. With decreasing temperature, they undergo sequential structural transitions from the cubic α phase to the tetragonal β phase at $\sim$280 K [29,30] and $\sim$250 K [31,32], then to the orthorhombic γ phase at $\sim$141 K [29,30] and $\sim$150 K [31,32], respectively. The transition from the α phase to the β phase is driven by tilting the MI$_6$ octahedrons. The tilting pattern of the PbI$_6$ octahedrons in FAPbI$_3$ is described in Glazer notation as $a^0a^0c^+$, which leads to the space group $P4/mbm$ in the β phase [33]. This result differs from the tilting pattern $a^0a^0c^-$ and the space group $I4/mcm$ in the β phase of MAPbI$_3$ [33]. Consequently, the lattice instability in the cubic phase of FAPbI$_3$ is larger at the M point than the R point (Fig. 1) in contrast to MAPbI$_3$. The space group in the β phase of FASnI$_3$ is the same as FAPbI$_3$ [31,32]. Note that the crystal structure and the space group of the γ phase in both compounds, and even structural transitions from the β phase in FAPbI$_3$ are still controversial [29–32].

II. EXPERIMENTAL DETAILS

A single crystal of FAPbI$_3$ with typical dimensions of $4 \times 4 \times 2$ mm^3 was synthesized by an inverse-temperature-crystallization method. A single crystal of FASnI$_3$ with typical dimensions of $0.3 \times 0.3 \times 0.3$ mm^3 was grown by the aqueous

solution process using phosphinic acid (H$_3$PO$_2$). Details of the crystal growth of the samples are described in the Supplemental Material [34]. We employ the cubic unit cell in this paper.

The IXS experiments were conducted at BL35XU of SPring-8 in Japan. Using a Si(11 11 11) backscattering, the incident x-ray energy was tuned to 21.747 keV with energy resolution of 1.5 meV. Resolutions of a momentum transfer in FAPbI$_3$ and FASnI$_3$ were (0.09, 0.09, 0.04) and (0.09, 0.09, 0.05) in reciprocal lattice units (r.l.u.). The sample temperature was controlled using a He closed-cycle refrigerator. The IXS experiments were performed at room temperature (RT) and 200 K for FAPbI$_3$ and RT and 180 K for FASnI$_3$, where both samples exhibited the α and β phases, respectively [29–31]. In our IXS measurements, the lattice constants a of FAPbI$_3$ and FASnI$_3$ are 6.360 Å and 6.315 Å at RT, and 6.311 Å at 200 K and 6.267 Å at 180 K, respectively, which are used to estimate mass densities and sound speeds. These values are consistent with those in the literature [27,29–31]. No x-ray damage to the samples could be seen during and after the IXS experiments. The phonon energies were obtained by fitting the measured IXS spectra using the Lorentz function with the Bose factor,

$$I(\mathbf{Q}, E) = I_e(\mathbf{Q}) + \sum_i I_i \frac{(\Gamma_i/2)^2}{(E \mp E_i)^2 + (\Gamma_i/2)^2}$$
$$\times (n(E_i) + 1/2 \pm 1/2)/E_i, \qquad (1)$$

where I_i, E_i, Γ_i, and $n(E)$ is the intensity, energy, the full width at half maximum of the phonon mode with index i, and the Bose factor, respectively. Upper and lower signs of $\mp$ ($\pm$) correspond to the energy loss side ($E > 0$) and the energy gain side ($E < 0$), respectively. The elastic part $I_e(\mathbf{Q})$ is also described by the Lorentz function, $I_e(\mathbf{Q}) = I'(\mathbf{Q})(\Gamma/2)^2/(E^2 + (\Gamma/2)^2)$. Taking the energy resolution into account, Γ is fixed as 1.5 meV.

A yellow polymorph of these compounds exists called the δ phase, as exemplified by δ-CsPbI$_3$ [35,36]. The yellow polymorph adopts the nonperovskite structure, which might be the most stable state in air [35,36]. However, the samples used in this study are black and as well-defined as the cubic perovskite structure at RT, even though the samples are exposed to air within a few hours for checking the principal axes of the crystals and the sample mounting before the IXS experiments. Moreover, they remain black for a few days even after the IXS experiments.

III. RESULTS AND DISCUSSION

Figures 2(a) and 2(b) show the typical IXS spectra of FAPbI$_3$ for the longitudinal mode along the Γ-M and Γ-X directions, respectively, at RT. These spectra ranging to 20 meV are considerably broad, and overall features in the transverse modes are similar. These features agree well with the previous studies on the lattice dynamics of the halide perovskites [37–46]. Figures 2(c) and 2(d) show similar datasets for FASnI$_3$. We find that the IXS spectra of FASnI$_3$ are also broad. Broad phonon spectra can be attributed to phonon anharmonicity [43,44], which also causes the short mean free paths of phonons, namely phonon glass behavior. Since the anharmonic potential creates an instant large atomic
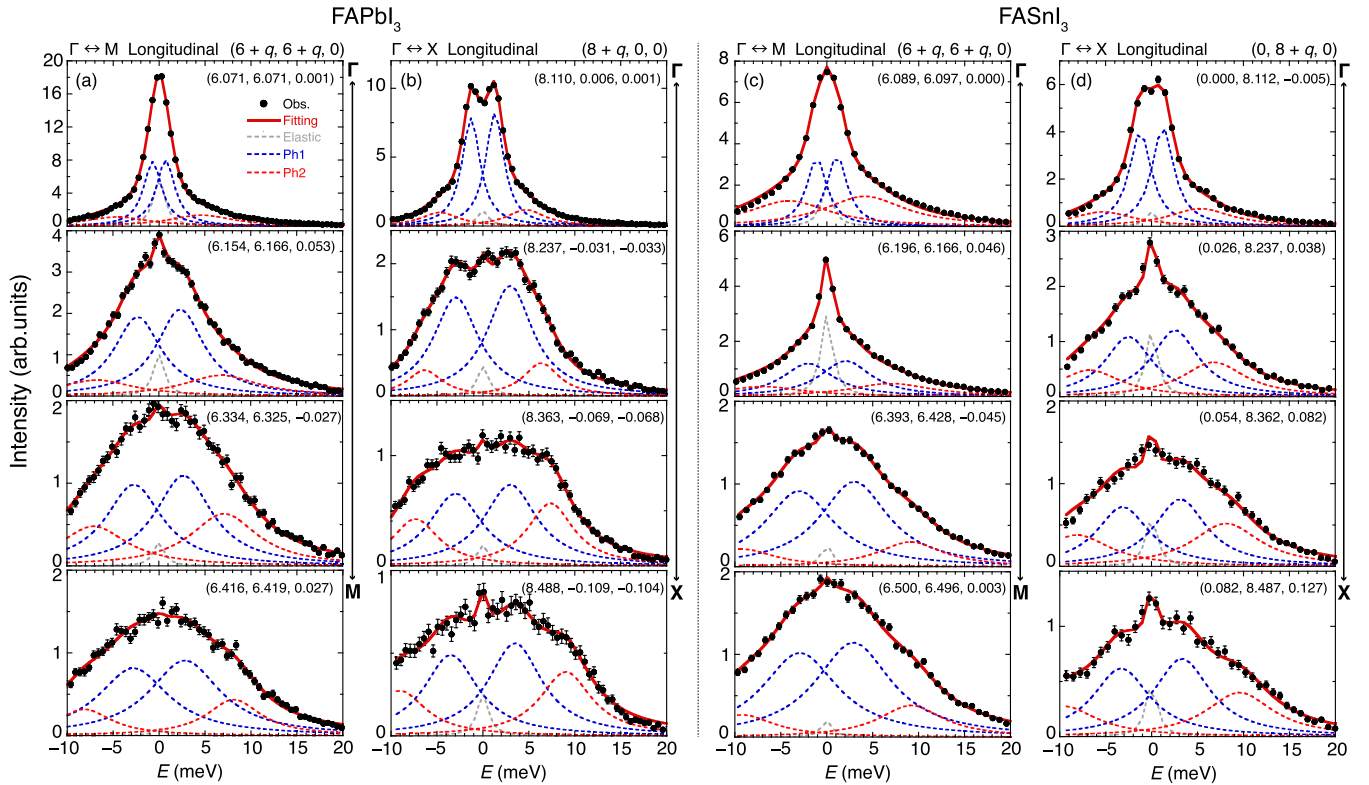
FIG. 2. Typical IXS spectra of (a), (b) FAPbI$_3$ and (c), (d) FASnI$_3$, at room temperature (RT), respectively. The data of panels (a) and (c) are measured at the longitudinal geometries along the Γ-M direction, and those of panels (b) and (d) are measured at the longitudinal geometries along the Γ-X direction.

displacement that can be coupled with the charge carriers, these broad phonon spectra due to phonon anharmonicity would be advantageous to the large polaron formation in the APbX$_3$ systems [7,45].

We estimate phonon energies by analyzing the measured IXS spectra using the Eq. (1). Figure 2 shows the fitted curves, thereby obtaining the phonon dispersion relations (Fig. 3). In these dispersion relations, quarter width at half maximum of phonon peaks are depicted as vertical bars instead of the fitting uncertainty. Although the overall dispersion relations are similar in FAPbI$_3$ and FASnI$_3$, a remarkable difference can be seen in the transverse mode with the [001] polarization along the Γ-M direction. In this mode, the energies of the lowest phonon excitations near the zone center in FASnI$_3$ are much smaller than those in FAPbI$_3$. This result is also evident from the spectra shown in Figs. 4(a) and 4(c). This result indicates that the speed of transverse sound along this direction in FASnI$_3$ is much smaller than in FAPbI$_3$, although the mass of Pb is two times larger than that of Sn. Note that the previous neutron scattering studies have reported quasielastic scatterings owing to the FA or MA molecular rotations, whose relaxation times are the order of nano second corresponding to the energy resolution of $1 \sim 10\,\mu$eV [37,47]. However, such a quasielastic scattering owing to the FA molecular rotations can not be extracted from our data, because the energy resolution of our IXS experiments is 1.5 meV and x-rays is not sensitive to the FA molecule. We estimate the speeds of sound and the elastic constants from the dispersion relations to extract the elastic properties of these systems. From a continuous approximation viewpoint, we use the longitudinal mode data along the Γ-X direction, the transverse mode data (the polarization is parallel to the [001] direction) along the Γ-M direction, and the longitudinal mode data along the Γ-M direction to calculate the speeds of sound, $v_{\mathrm{LA}}^{\Gamma X}$, $v_{\mathrm{TA}}^{\Gamma M}$, and $v_{\mathrm{LA}}^{\Gamma M}$, respectively. For the cubic lattice, the elastic constants are related to the speeds of sound as follows [50]: $v_{\mathrm{LA}}^{\Gamma X} = \sqrt{C_{11}/\rho}$, $v_{\mathrm{TA}}^{\Gamma M} = \sqrt{C_{44}/\rho}$, and $v_{\mathrm{LA}}^{\Gamma M} = \sqrt{(C_{11} + 2C_{44} + C_{12})/\rho}$, where ρ is the mass density. Table I summarizes the estimated speeds of sound and Table II provides the estimated elastic constants. To see the temperature variation, the speeds of sound and the elastic constants in the β phase are also estimated using the cubic notation.

The elastic constants of FAPbI$_3$ at RT, except for C_{44}, agree well with a previous report [42]. Also, these constants within the uncertainties satisfy the so-called Born stability criteria, the generic requirement for the elastic stability of cubic crystals [42,50,51]: $C_{11} > 0$, $C_{44} > 0$, $C_{11} - C_{12} > 0$, $C_{11} + 2C_{12} > 0$. A previous study reported that C_{44} of MAPbBr$_3$ smoothly decreases with the decreasing temperature from RT [42]. Accordingly, C_{44} of FAPbI$_3$ at 200 K in our data reduces significantly, also apparent from the IXS spectra shown in Figs. 4(a) and 4(b), and its value is consistent with previous results. Therefore, the larger C_{44} of FAPbI$_3$ at RT than in the previous one might result from the slight difference of the measurement temperature. We add that the lower q-resolution of our data than that in Ref. [42] may lead to larger differences in the speeds of sound and the elastic constants beyond the fitting errors for the broad peaks.
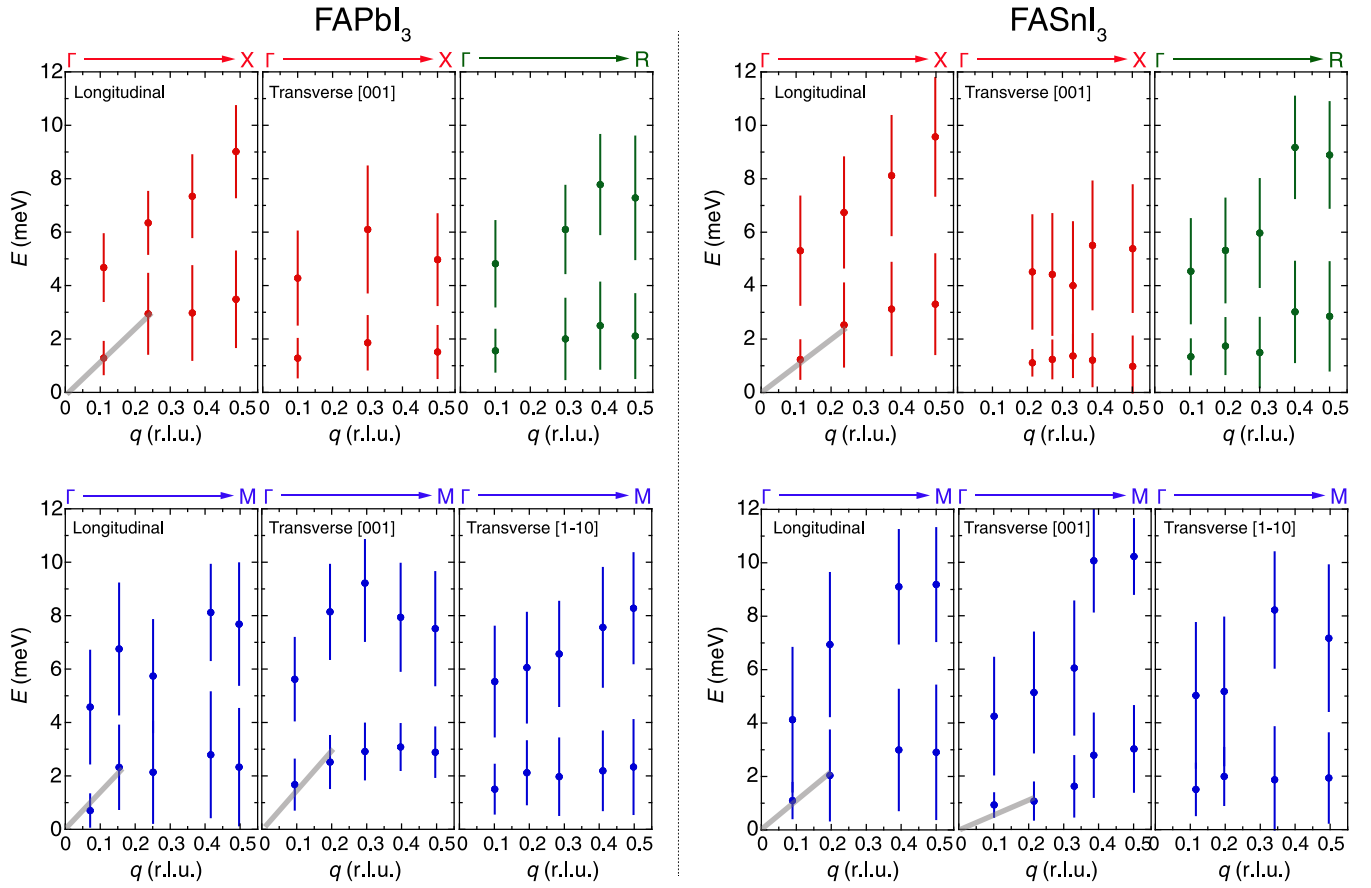
FAPbI₃

FASnI₃

FIG. 3. Phonon dispersion relations along the Γ-X (red), Γ-M (blue), and Γ-R (green) directions in FAPbI₃ (left panels) and FASnI₃ (right panels), respectively, at RT. Note that (i) the data along the Γ-R direction correspond to neither longitudinal nor transverse modes because of the scattering geometry, and (ii) the vertical bars are quarter width at half maximum phonon peaks, not the uncertainty of fitting; the gray solid lines are a guide for the eyes.
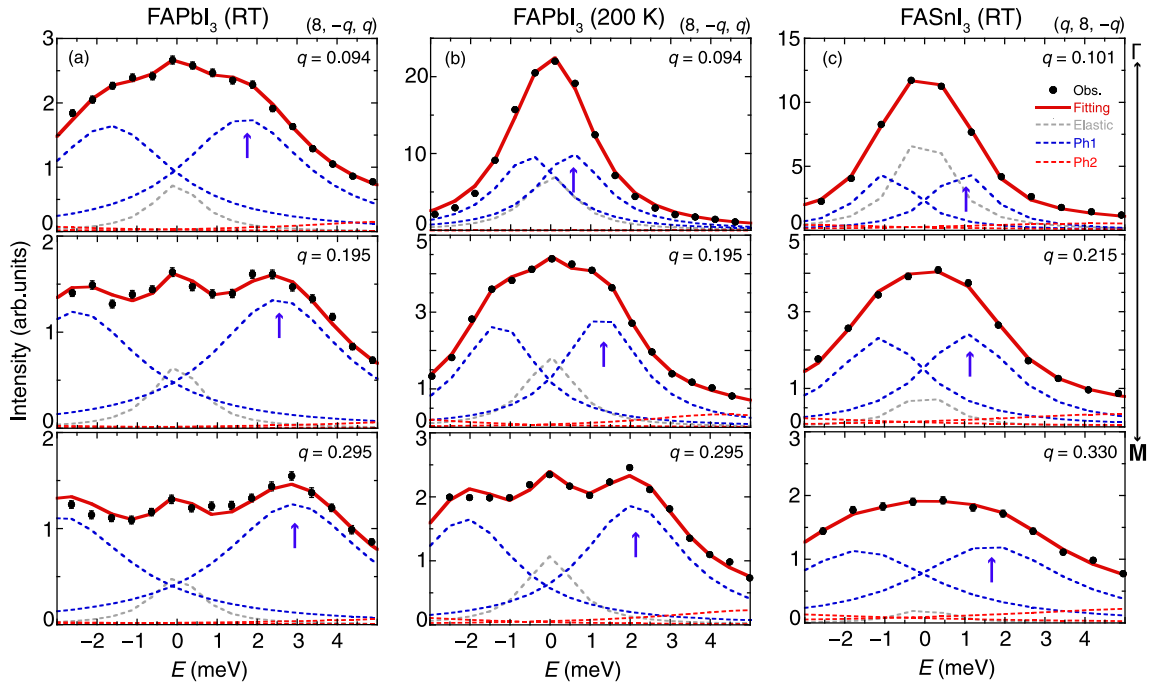

FIG. 4. IXS spectra in the range relevant to the sound velocity for the transverse [001] mode along the Γ-M direction in (a) FAPbI₃ at RT, (b) FAPbI₃ at 200 K, and (c) FASnI₃ at RT.

TABLE I. Speeds of sound estimated in FAPbI$_3$ and FASnI$_3$; all values are given in m/s.

	Temperature	$v_{LA}^{\Gamma X}$	$v_{TA}^{\Gamma M}$	$v_{LA}^{\Gamma M}$
FAPbI$_3$	RT (Cubic α phase)	2000 ± 120	1400 ± 80	1500 ± 150
	200 K (Tetragonal β phase)	1730 ± 70	690 ± 30	1200 ± 100
FASnI$_3$	RT (Cubic α phase)	1890 ± 60	600 ± 90	1170 ± 90
	180 K (Tetragonal β phase)	1430 ± 80	610 ± 80	1100 ± 100

As expected from the IXS spectra shown in Fig. 4, the C_{44} of FASnI$_3$ at RT is significantly smaller than that of FAPbI$_3$. Furthermore, the absolute values of the other elastic constants of FASnI$_3$ are smaller than those of FAPbI$_3$, although the error margin is large. The result correlates well with the theoretical prediction, showing that the Pb-I bonds in FAPbI$_3$ are stronger than the Sn-I bonds in FASnI$_3$ [48]. This result suggests that the solid state stability of FASnI$_3$ is less than that of FAPbI$_3$. The single crystal of FASnI$_3$ prepared in this study is very small in size as described in Sec. II, whereas the large single crystal of FAPbI$_3$ is available. As well as the elastic constants, the speeds of sound of FASnI$_3$ are smaller than those of FAPbI$_3$. In addition, no significant difference in the phonon lifetimes (the reciprocal of the width of the phonon peaks) of FAPbI$_3$ and FASnI$_3$ is observed in our data. Since the lattice thermal conductivity is proportional to the speeds of sound (phonon group velocities) and the phonon lifetime, these lower speeds of sound would directly correspond to the lower lattice thermal conductivity of ASnX$_3$ than its APbX$_3$ counterparts [8,28]. Note that the width of the acoustic phonon peaks tend to become broader near the zone boundaries in both FAPbI$_3$ and FASnI$_3$. This tendency is also reported for the several metal halide perovskites [39,41,43,52,53], in which the importance of the contribution from the A site molecules is suggested, such as the molecular dynamics through the hydrogen bonding [54] or anharmonic effect due to low energy optical modes arising from the A site molecules [43]. However, Songvilay et al. have recently demonstrated that the width of the acoustic phonons are similar in MAPbCl$_3$ and CsPbBr$_3$, which indicates that the role of the organic molecules and the difference in the halide X$^-$ ions are not crucial for the broadening of the acoustic phonon peaks [52]. Taking this study into account, there are possibility that the difference in the Pb^{2+} and Sn^{2+} ions also does not affect the acoustic phonon lifetimes in FAPbI$_3$ and FASnI$_3$.

As briefly described in Sec. I, the microscopic origin of the long carrier lifetime in this system must be elucidated more clearly for photovoltaic and optoelectronic applications. Several explanations for the long relaxation time have been proposed, including the (dynamical) Rashba effect [55–57] and the large polaron formation [12–17]. Moreover, the phonon bottleneck effect occurs in this system at higher carrier densities [18–23]. Some mechanisms stated above could coexist with the phonon bottleneck effect and might cowork to elongate the relaxation, because there are several characteristic time scales in the relaxation process of the hot carriers [20–22]. The phonon bottleneck effect indicates some factors due to phonons that hinder the energy dissipation of the hot carriers. As one of the possible origins of the phonon bottleneck effect, Yang et al. proposed the up-conversion mechanism of low-energy acoustic phonons [20]. In this mechanism, it is assumed that blocking acoustic phonon propagation due to anharmonic scattering suppresses thermal transport and thermal (vibrational) energy dissipation, and then the recycled vibrational energy reheats the carries [20]. As highlighted in the literature [20,22,24], this up-conversion of acoustic phonons occurs easily in materials with lower lattice thermal conductivity, where acoustic phonon propagation is more strongly prevented. This assumption is in line with the lower thermal conductivity of FASnI$_3$, corroborated by our results that the speeds of sound in FASnI$_3$ are lower than in FAPbI$_3$, and the resulting longer relaxation time in FASnI$_3$ [22,24]. Therefore, in terms of their mechanical properties, our results favor the up-conversion mechanism, where acoustic phonon modes are involved.

Another explanation exists for the phonon bottleneck effect, and thus, the origin of the phonon bottleneck effect is still controversial. For example, Fu et al. have proposed that at moderate carrier densities, the bottleneck effect results from the suppression of the Klemens relaxation which involves the longitudinal optical (LO) phonon decay. At higher carrier densities, the Auger heating process occurs and further

TABLE II. Elastic constants and bulk moduli B of FAPbI$_3$ and FASnI$_3$; all values are given in GPa.

	Temperature (phase or structure)	C_{11}	C_{44}	C_{12}	$B = (C_{11} + 2C_{12})/3$
FAPbI$_3$	RT (α phase)	15.9 ± 3.9	8.0 ± 1.8	-12.4 ± 6.6	-2.9 ± 4.6
	200 K (β phase)	12.5 ± 1.0	2.0 ± 0.2	-3.5 ± 2.5	1.8 ± 1.7
FASnI$_3$	RT (α phase)	12.9 ± 1.6	1.3 ± 0.8	-5.6 ± 3.5	0.5 ± 2.4
	180 K (β phase)	7.6 ± 0.8	1.4 ± 0.4	-1.8 ± 2.3	1.3 ± 1.6
FAPbI$_3$ [42]	RT (α phase)	11.1 ± 2.0	2.7 ± 0.3	-5.5 ± 2.2	0.0 ± 2.4
FAPbI$_3$ (Calc.) [48]	(a pseudo-cubic structure)	30.15	2.03	2.99	13.25
FAPbI$_3$ (Calc.) [49]	(the cubic structure)	20.5	4.8	12.3	15.3
FASnI$_3$ (Calc.) [48]	(a pseudo-cubic structure)	29.96	2.35	6.85	12.96

reduces the cooling rate [21]. However, Sekiguchi *et al.* recently provided direct evidence of the phonon bottleneck effect, where the excitation of transverse optical (TO) phonons by a terahertz pulse laser elongates the carrier lifetime [23]. Since the Fröhlich interaction between carriers and the LO phonons is dominant in these materials [58–60], they argued that the up-conversion from the excited TO phonons to LO phonons possibly occurs [23]. Although it is still unclear whether the up-conversion from excited TO phonons to LO phonons occurs directly or through the acoustic phonons [23], some up-conversion might occur between phonons in the metal halide perovskites.

In general, the elastic constants increase with decreasing temperature [50], corresponding to the hardening of a solid as the temperature decreases. As shown in Table II, the C_{44} of FAPbI$_3$ shows an opposite temperature dependence, whereas that of FASnI$_3$ is almost unchanged. As described above, this tendency has also been reported in MAPbBr$_3$ [42]. The authors of the literature [42] highlighted that this softening of C_{44} is related to the proximity of a ferroelastic transition [61], but it is independent of the cubic-to-tetragonal transition. The change in C_{44} of MAPbBr$_3$ weakens before the phase transition from the cubic α to the tetragonal β phases, or rather it is blocked by the cubic-to-tetragonal transition. The lower variation in C_{44} of FASnI$_3$ might be due to a similar situation, which would result from the lower cubic-to-tetragonal transition temperature. It is helpful to measure the elastic constants of FASnI$_3$ at higher temperatures to confirm this point. We add that the temperature dependence of C_{11} of FASnI$_3$ also contradicts the general tendency, whereas that of FAPbI$_3$ is unclear due to the large uncertainties.

Finally, we compare the elastic constants deduced by the experiments with those of the calculations. Table II shows that the calculations estimate that C_{11} is larger than the experiments. Also, a significant difference exists between the experimental and calculated results of C_{12} in both compounds [48,49]. First-principles calculations for the instability of tilting the MX$_6$ octahedron in CsMX$_3$ revealed that the cubic structure is realized as a time-average structure due to the dynamical disorder of the octahedral tilting [9,10]. Subsequently, the dynamical disorder of the octahedral tilting was experimentally verified in CsPbBr$_3$ [46], which would be a common feature in the metal halide perovskites. Therefore, the discrepancy in the elastic constants might be due to the use of the static cubic structure in the calculations. We note that the negative values of C_{12} are seen only in FAPbI$_3$ and FASnI$_3$ among the metal halide perovskites. Combining FA and I, which are common to both compounds, might enhance the dynamical disorder of the octahedron.

IV. SUMMARY AND CONCLUSIONS

We performed IXS experiments to investigate the lattice dynamics of FAPbI$_3$ and FASnI$_3$ in their cubic α and tetragonal β phases. The speeds of sound and elastic constants of FASnI$_3$ are smaller than those of FAPbI$_3$ in both phases. These results corroborate the reported tendency that the thermal conductivity and the hot carrier lifetime of ASnX$_3$ are lower and longer, respectively, than those of APbX$_3$. Our results also favor the up-conversion mechanism by acoustic phonons in the phonon bottleneck effect observed in the metal halide perovskites. A more sophisticated theoretical calculation for the elastic constants, which might need to include the effect of the dynamical disorder of the MX$_6$ octahedron, is desirable.

[1] S. D. Stranks and H. J. Snaith, Nat. Nanotechnol. **10**, 391 (2015).

[2] T. M. Brenner, D. A. Egger, L. Kronik, G. Hodes, and D. Cahen, Nat. Rev. Mater. **1**, 15007 (2016).

[3] M. A. Haque, S. Kee, D. R. Villalva, W.-L. Ong, and D. Baran, Adv. Sci. **7**, 1903389 (2020).

[4] A. K. Baranwal and S. Hayase, Nanomater. **12**, 4055 (2022).

[5] A. Kojima, K. Teshima, Y. Shirai, and T. Miyasaka, J. Am. Chem. Soc. **131**, 6050 (2009).

[6] G. A. Slack, New materials and performance limits for thermoelectric cooling, in *CRC Handbook of Thermoelectrics* (CRC Press, Boca Raton, FL,1995).

[7] K. Miyata, T. L. Atallah, and X.-Y. Zhu, Sci. Adv. **3**, e1701469 (2017).

[8] W. Lee, H. Li, A. B. Wong, D. Zhang, M. Lai, Y. Yu, Q. Kong, E. Lin, J. J. Urban, J. C. Grossman, and P. Yang, Proc. Natl. Acad. Sci. USA **114**, 8693 (2017).

[9] R. X. Yang, J. M. Skelton, E. L. da Silva, J. M. Frost, and A. Walsh, J. Phys. Chem. Lett. **8**, 4720 (2017).

[10] J. Klarbring, Phys. Rev. B **99**, 104105 (2019).

[11] T. Hata, G. Giorgi, and K. Yamashita, Nano Lett. **16**, 2749 (2016).

[12] X.-Y. Zhu and V. Podzorov, J. Phys. Chem. Lett. **6**, 4758 (2015).

[13] H. Zhu, K. Miyata, Y. Fu, J. Wang, P. P. Joshi, D. Niesner, K. W. Williams, S. Jin, and X.-Y. Zhu, Science **353**, 1409 (2016).

[14] T. Chen, W.-L. Chen, B. J. Foley, J. Lee, J. P. C. Ruff, J. Y. P. Ko, C. M. Brown, L. W. Harriger, D. Zhang, C. Park, M. Yoon, Y.-M. Chang, J. J. Choi, and S.-H. Lee, Proc. Natl. Acad. Sci. USA **114**, 7519 (2017).

[15] M. Puppin, S. Polishchuk, N. Colonna, A. Crepaldi, D. N. Dirin, O. Nazarenko, R. De Gennaro, G. Gatti, S. Roth, T. Barillot, L. Poletto, R. P. Xian, L. Rettig, M. Wolf, R. Ernstorfer, M. V. Kovalenko, N. Marzari, M. Grioni, and M. Chergui, Phys. Rev. Lett. **124**, 206402 (2020).

[16] B. Guzelturk, T. Winkler, T. W. J. Van de Goor, M. D. Smith, S. A. Bourelle, S. Feldmann, M. Trigo, S. W. Teitelbaum, H.-G. Steinrück, G. A. de la Pena, R. Alonso-Mori, D. Zhu, T. Sato, H. I. Karunadasa, M. F. Toney, F. Deschler, and A. M. Lindenberg, Nat. Mater. **20**, 618 (2021).

[17] X. Yue, C. Wang, B. Zhang, Z. Zhang, Z. Xiong, X. Zu, Z. Liu, Z. Hu, G. O. Odunmbaku, Y. Zheng, K. Sun, and J. Du, Nat. Commun. **14**, 917 (2023).

[18] M. B. Price, J. Butkus, T. C. Jellicoe, A. Sadhanala, A. Briane, J. E. Halpert, K. Broch, J. M. Hodgkiss, R. H. Friend, and F. Deschler, Nat. Commun. **6**, 8420 (2015).

[19] Y. Yang, D. P. Ostrowski, R. M. France, K. Zhu, J. van de Lagemaat, J. M. Luther, and M. C. Beard, Nat. Photon. **10**, 53 (2016).

[20] J. Yang, X. Wen, H. Xia, R. Sheng, Q. Ma, J. Kim, P. Tapping, T. Harada, T. W. Kee, F. Huang, Y.-B. Cheng, M. Green, A. Ho-Baillie, S. Huang, S. Shrestha, R. Patterson, and G. Conibeer, Nat. Commun. **8**, 14120 (2017).

[21] J. Fu, Q. Xu, G. Han, B. Wu, C. H. A. Huan, M. L. Leek, and T. C. Sum, Nat. Commun. **8**, 1300 (2017).

[22] H.-H. Fang, S. Adjokatse, S. Shao, J. Even, and M. A. Loi, Nat. Commun. **9**, 243 (2018).

[23] F. Sekiguchi, H. Hirori, G. Yumoto, A. Shimazaki, T. Nakamura, A. Wakamiya, and Y. Kanemitsu, Phys. Rev. Lett. **126**, 077401 (2021).

[24] S. Kahmann and M. A. Loi, J. Mater. Chem. C **7**, 2471 (2019).

[25] M. Konstantakou and T. Stergiopoulos, J. Mater. Chem. A **5**, 11518 (2017).

[26] W. Ke, C. C. Stoumpos, and M. G. Kanatzidis, Adv. Mater. **31**, 1803230 (2019).

[27] L. He, H. Gu, X. Liu, P. Li, Y. Dang, C. Liang, L. K. Ono, Y. Qi, and X. Tao, Matter **2**, 167 (2020).

[28] X. Mettan, R. Pisoni, P. Matus, A. Pisoni, J. Jaćimović, B. Náfrádi, M. Spina, D. Pavuna, L. Forró, and E. Horváth, J. Phys. Chem. C **119**, 11506 (2015).

[29] D. H. Fabini, C. C. Stoumpos, G. Laurita, A. Kaltzoglou, A. G. Kontos, P. Falaras, M. G. Kanatzidis, and R. Seshadri, Angew. Chem. Int. Ed. **55**, 15392 (2016).

[30] S. Kawachi, M. Atsumi, N. Saito, N. Ohashi, Y. Murakami, and J. Yamaura, J. Phys. Chem. Lett. **10**, 6967 (2019).

[31] E. C. Schueller, G. Laurita, D. H. Fabini, C. C. Stoumpos, M. G. Kanatzidis, and R. Seshadri, Inorg. Chem. **57**, 695 (2018).

[32] S. Kahmann, O. Nazarenko, S. Shao, O. Hordiichuk, M. Kepenekian, J. Even, M. V. Kovalenko, G. R. Blake, and M. A. Loi, ACS Energy Lett. **5**, 2512 (2020).

[33] D. H. Fabini, T. A. Siaw, C. C. Stoumpos, G. Laurita, D. Olds, K. Page, J. G. Hu, M. G. Kanatzidis, S. Han, and R. Seshadri, J. Am. Chem. Soc. **139**, 16875 (2017).

[34] See Supplemental Material at http://link.aps.org/supplemental/10.1103/PhysRevB.110.024301 for the details of the crystal growth of the samples. The Supplemental Material also includes Refs. [62–64].

[35] S. Dastidar, C. J. Hawley, A. D. Dillon, A. D. Gutierrez-Perez, J. E. Spanier, and A. T. Fafarman, J. Phys. Chem. Lett. **8**, 1278 (2017).

[36] R. J. Sutton, M. R. Filip, A. A. Haghighirad, N. Sakai, B. Wenger, F. Giustino, and H. J. Snaith, ACS Energy Lett. **3**, 1787 (2018).

[37] I. P. Swainson, C. Stock, S. F. Parker, L. Van Eijck, M. Russina, and J. W. Taylor, Phys. Rev. B **92**, 100303(R) (2015).

[38] A. Létoublon, S. Paofai, B. Rufflé, P. Bourges, B. Hehlen, T. Michel, C. Ecolivet, O. Durand, S. Cordier, C. Katan, and J. Even, J. Phys. Chem. Lett. **7**, 3776 (2016).

[39] R. Comin, M. K. Crawford, A. H. Said, N. Herron, W. E. Guise, X. Wang, P. S. Whitfield, A. Jain, X. Gong, A. J. H. McGaughey, and E. H. Sargent, Phys. Rev. B **94**, 094301 (2016).

[40] A. N. Beecher, O. E. Semonin, J. M. Skelton, J. M. Frost, M. W. Terban, H. Zhai, A. Alatas, J. S. Owen, A. Walsh, and S. J. L. Billinge, ACS Energy Lett. **1**, 880 (2016).

[41] M. Songvilay, M. Bari, Z.-G. Ye, G. Xu, P. M. Gehring, W. D. Ratcliff, K. Schmalzl, F. Bourdarot, B. Roessli, and C. Stock, Phys. Rev. Mater. **2**, 123601 (2018).

[42] A. C. Ferreira, A. Létoublon, S. Paofai, S. Raymond, C. Ecolivet, B. Rufflé, S. Cordier, C. Katan, M. I. Saidaminov, A. A. Zhumekenov, O. M. Bakr, J. Even, and P. Bourges, Phys. Rev. Lett. **121**, 085502 (2018).

[43] A. Gold-Parker, P. M. Gehring, J. M. Skelton, I. C. Smith, D. Parshall, J. M. Frost, H. I. Karunadasa, A. Walsh, and M. F. Toney, Proc. Natl. Acad. Sci. USA **115**, 11905 (2018).

[44] A. C. Ferreira, S. Paofai, A. Létoublon, J. Ollivier, S. Raymond, B. Hehlen, B. Rufflé, S. Cordier, C. Katan, J. Even, and P. Bourges, Commun. Phys. **3**, 48 (2020).

[45] D. Zhang, X. Hu, T. Chen, D. L. Abernathy, R. Kajimoto, M. Nakamura, M. Kofu, B. J. Foley, M. Yoon, J. J. Choi, and S.-H. Lee, Phys. Rev. B **102**, 224310 (2020).

[46] T. Lanigan-Atkins, X. He, M. J. Krogstad, D. M. Pajerowski, D. L. Abernathy, G. N. M. N. Xu, Z. Xu, D.-Y. Chung, M. G. Kanatzidis, S. Rosenkranz, R. Osborn, and O. Delaire, Nat. Mater. **20**, 977 (2021).

[47] B. Li, Y. Kawakita, Y. Liu, M. Wang, M. Matsuura, K. Shibata, S. Ohira-Kawamura, T. Yamada, S. Lin, K. Nakajima, and S. F. Liu, Nat. Commun. **8**, 16086 (2017).

[48] L. Guo, G. Tang, and J. Hong, Chin. Phys. Lett. **36**, 056201 (2019).

[49] J.-F. Wang, X.-N. Fu, and J.-T. Wang, Chin. Phys. B **26**, 106301 (2017).

[50] C. Kittel, *Introduction to Solid State Physics*, 8th ed. (John Wiley & Sons, New York, NY, 2005).

[51] F. Mouhat and F.-X. Coudert, Phys. Rev. B **90**, 224104 (2014).

[52] M. Songvilay, N. Giles-Donovan, M. Bari, Z.-G. Ye, J. L. Minns, M. A. Green, G. Xu, P. M. Gehring, K. Schmalzl, W. D. Ratcliff, C. M. Brown, D. Chernyshov, W. van Beek, S. Cochran, and C. Stock, Phys. Rev. Mater. **3**, 093602 (2019).

[53] M. E. Manley, K. Hong, P. Yin, S. Chi, Y. Cai, C. Hua, L. L. Daemen, R. P. Hermann, H. Wang, A. F. May, M. Asta, and M. Ahmadi, Sci. Adv. **6**, eaaz1842 (2020).

[54] S.-Y. Yue, X. Zhang, G. Qin, J. Yang, and M. Hu, Phys. Rev. B **94**, 115427 (2016).

[55] T. Etienne, E. Mosconi, and F. De Angelis, J. Phys. Chem. Lett. **7**, 1638 (2016).

[56] E. M. Hutter, M. C. Gélvez-Rueda, A. Osherov, V. Bulović, F. C. Grozema, S. D. Stranks, and T. J. Savenije, Nat. Mater. **16**, 115 (2017).

[57] B. Wu, H. Yuan, Q. Xu, J. A. Steele, D. Giovanni, P. Puech, J. Fu, Y. F. Ng, N. F. Jamaludin, A. Solanki, S. Mhaisalkar, N. Mathews, M. B. J. Roeffaers, M. Grätzel, J. Hofkens, and T. C. Sum, Nat. Commun. **10**, 484 (2019).

[58] A. D. Wright, C. Verdi, R. L. Milot, G. E. Eperon, M. A. Pérez-Osorio, H. J. Snaith, F. Giustino, M. B. Johnston, and L. M. Herz, Nat. Commun. **7**, 11755 (2016).

[59] C. M. Iaru, J. J. Geuchies, P. M. Koenraad, D. Vanmaekelbergh, and A. Y. Silov, ACS Nano **11**, 11024 (2017).

[60] M. Schlipf, S. Poncé, and F. Giustino, Phys. Rev. Lett. **121**, 086402 (2018).

[61] Y. Liu, L. Collins, R. Proksch, S. Kim, B. R. Watson, B. Doughty, T. R. Calhoun, M. Ahmadi, A. V. Ievlev, S. Jesse, S. T. Retterer, A. Belianinov, K. Xiao, J. Huang, B. G. Sumpter, S. V. Kalinin, B. Hu, and O. S. Ovchinnikova, Nat. Mater. **17**, 1013 (2018).

[62] M. I. Saidaminov, A. L. Abdelhady, G. Maculan, and O. M. Bakr, Chem. Commun. **51**, 17658 (2015).

[63] Y. Dang, Y. Zhou, X. Liu, D. Ju, S. Xia, H. Xia, and X. Tao, Angew. Chem. Int. Ed. **55**, 3447 (2016).

[64] N. Ohashi, Y. Matsushita, and N. Saito, J. Solid State Chem. **306**, 122778 (2022).